

# MOND orbits in the Oort cloud

L. Iorio

*INFN-Sezione di Pisa. Address for correspondence: Viale Unità di Italia 68  
70125 Bari, Italy*

*tel. 0039 328 6128815*

*e-mail: lorenzo.iorio@libero.it*

## Abstract

We numerically investigate the features of typical orbits occurring in the Oort cloud ( $r \approx 50 - 150$  kAU) in the low-acceleration regime of the MODified Newtonian Dynamics (MOND) taking into account the External Field Effect (EFE). We use three different forms of the MOND interpolating function  $\mu(x)$  and two different values for the Galactic field at the Sun's location. We find that MOND produces highly distorted trajectories with respect to the Newtonian case, especially for very eccentric orbits: in particular, the MOND paths in the ecliptic plane get shrunk extending over much smaller spatial regions than the Newtonian case, and experience high frequency variations over one Keplerian orbital period. This fact may have consequences on the composition and the dynamical history of the Oort cloud since the perturbations due to nearby passing stars, interstellar gas clouds and Galactic tides, which in the classical framework change the velocities of the Oort's comets launching them in the inner regions of the Solar System, might be less effective according to MOND. The nearly polar orbits are distorted as well, but they occupy more extended spatial regions with respect to the ecliptic case.

Keywords: Modified theories of gravity- Celestial mechanics- Oort cloud  
PACS 04.50.Kd; 95.10.Ce; 96.50.Hp

## 1 Introduction

In many astrophysical systems like, e.g., spiral galaxies and clusters of galaxies a discrepancy between the observed kinematics of their exterior parts and the predicted one on the basis of the Newtonian dynamics and the matter detected from the emitted electromagnetic radiation (visible stars and gas clouds) was present since the pioneering studies by Bosma [1] and Rubin and coworkers [2] on spiral galaxies. More precisely, such an effect shows up in the galactic velocity rotation curves whose typical pattern after a few

kpc from the center differs from the Keplerian  $1/\sqrt{r}$  fall-off expected from the usual dynamics applied to the electromagnetically-observed matter.

As a possible solution of this puzzle, the existence of non-baryonic, weakly-interacting Cold Dark (in the sense that its existence is indirectly inferred only from its gravitational action, not from emitted electromagnetic radiation) Matter (CDM) was proposed to reconcile the predictions with the observations [3] in the framework of the standard gravitational physics.

Oppositely, it was postulated that the Newtonian laws of gravitation may have to be modified on certain acceleration scales to correctly account for the observed anomalous kinematics of such astrophysical systems without resorting to still undetected exotic forms of matter. One of the most phenomenologically successful modification of the inverse-square Newtonian law, mainly with respect to spiral galaxies, is the MODified Newtonian Dynamics (MOND) [4, 5, 6] which postulates that for systems experiencing total gravitational acceleration  $A < A_0$ , with [7]

$$A_0 = (1.2 \pm 0.27) \times 10^{-10} \text{ m s}^{-2}, \quad (1)$$

$$\mathbf{A} \rightarrow \mathbf{A}_{\text{MOND}} = -\frac{\sqrt{A_0 GM}}{r} \hat{\mathbf{r}}. \quad (2)$$

More precisely, it holds

$$A = \frac{N}{\mu(x)}, \quad x \equiv \frac{A}{A_0}; \quad (3)$$

$\mu(x) \rightarrow 1$  for  $x \gg 1$ , i.e. for large accelerations (with respect to  $A_0$ ), while  $\mu(x) \rightarrow x$  yielding eq. (2) for  $x \ll 1$ , i.e. for small accelerations. The most widely used forms for the interpolating function  $\mu$  are

$$\mu_1(x) = \frac{x}{1+x}, \quad [8] \quad (4)$$

$$\mu_2(x) = \frac{x}{(1+x^2)^{1/2}} \quad [9]. \quad (5)$$

Such forms, and also others, as we will see later, can be reduced to the following high-acceleration limit ( $x \gg 1$ )

$$\mu \approx 1 - k_0 x^{-\alpha}. \quad (6)$$

Indeed, eq. (4) corresponds to  $k_0 = 1$ ,  $\alpha = 1$ , while eq. (5) corresponds to  $k_0 = 1/2$  and  $\alpha = 2$ . It recently turned out that the simpler form of eq. (4) yields better results in fitting the terminal velocity curve of the Milky Way,

the rotation curve of the standard external galaxy NGC 3198 [8, 10, 11] and of a sample of 17 high surface brightness, early-type disc galaxies [12]. Eq. (3) strictly holds for co-planar, spherically and axially symmetric isolated mass distributions [13]; otherwise, the full modified (non-relativistic) Poisson equation [9]

$$\nabla \cdot \left[ \mu \left( \frac{|\nabla U|}{A_0} \right) \nabla U \right] = 4\pi G\rho, \quad (7)$$

where  $U$  is the gravitational potential,  $G$  is the Newtonian constant of gravitation and  $\rho$  is the matter density, must be used. In the Solar System the aforementioned symmetry conditions holds, so that we will use eq. (3), as done by a number of other authors [4, 23, 24, 28]. From the phenomenological point of view, the existence of a constant and uniform non-vanishing curl term breaking the symmetry has been recently constrained down to  $10^{-14}$  m s $^{-2}$  level with the perihelion precessions of the inner planets [17].

Attempts to yield a physical foundation to MOND, especially in terms of a relativistic covariant theory, can be found in, e.g., [14, 15, 16]; for recent reviews of various aspects of the MOND paradigm, see [18, 19, 20].

After setting the theoretical background which we will use in the rest of the paper, we will explore the strong MONDian regime in the remote ( $r = 50 - 150$  kAU) periphery of the Solar System, where the Oort cloud [21], populated by a huge number of small bodies moving along very eccentric and inclined to the ecliptic orbits, is supposed to exist; for preliminary investigations on such a topic, see Ref. [4, 22]. In particular, we will numerically investigate the modifications that MOND would induce on the Newtonian orbits of a test particle moving in such a region; this will allow us to put forth some hypothesis on the overall configuration that the Oort cloud would have if MOND was valid. We will also have to consider the subtle External Field Effect (EFE) which, in MOND, takes into account the influence of the Galactic field in the inner dynamics of the solar system.

For other works on MOND in the inner regions of the solar system, see Ref. [4, 23, 24, 25, 26, 27, 28, 29, 30, 31].

## 2 The External Field Effect in MOND

In the framework of MOND, the internal dynamics of a gravitating system  $S$  embedded in a larger one  $S$  is affected by the external background field  $E$  of  $S$  even if it is constant and uniform, thus implying a violation of the Strong Equivalence Principle: it is the so-called External Field Effect (EFE). In the case of the solar system,  $E$  would be  $A_{\text{cen}} \approx 10^{-10}$  m s $^{-2}$  because of

its motion through the Milky Way [4, 9, 22]. Clarifying EFE's concrete effects on the orbital dynamics of  $s$  is not an easy task; the existence in the inner regions of the solar system of its simplest form, i.e. a constant and uniform vector field  $\mathbf{E}$  with  $E \approx 10^{-10} \text{ m s}^{-2}$ , has been recently ruled out [17]. Milgrom in [30] has put forth a different form for the planetary EFE yielding a quadrupolar acceleration which mimics the action of distant mass; some consequences have been investigated in [31].

Moving to the remote periphery of the solar system, let us define the following quantities

$$\eta = \frac{A_{\text{cen}}}{A_0} \gtrsim 1, \quad (8)$$

$$r_t = \sqrt{\frac{GM}{A_0}} = 6.833 \text{ kAU}, \quad (9)$$

$$L = \frac{x}{\mu} \left( \frac{d\mu}{dx} \right), \quad (10)$$

$$\mu_g = \mu(\eta), \quad (11)$$

$$L_g = L(\eta). \quad (12)$$

In the weak acceleration regime, for

$$r \gg r_t \eta^{-1/2}, \quad (13)$$

i.e. in the Oort cloud, the action of EFE is different, so that the acceleration felt by an Oort comet is [9, 30]

$$\mathbf{A} = -\frac{GM}{\mu_g(1+L_g)^{1/2}} \left( \frac{x^2}{1+L_g} + y^2 + z^2 \right)^{-3/2} \begin{pmatrix} \frac{x}{1+L_g} \\ y \\ z \end{pmatrix}. \quad (14)$$

Note that, since the ecliptic longitude and latitude of the Galactic Center are about  $\lambda_{\text{GC}} \approx 180 \text{ deg}$ ,  $\beta_{\text{GC}} \approx -6 \text{ deg}$  [31], EFE is directed along the  $X$  axis of the ICRF, i.e. the barycentric frame in which the motion of solar system's objects are usually studied.

Concerning  $L$ , we have

$$\mu_1 = \frac{x}{1+x} \rightarrow L_1 = \frac{1}{1+x}, \quad (15)$$

$$\mu_2 = \frac{x}{(1+x^2)^{1/2}} \rightarrow L_2 = \frac{1}{1+x^2}, \quad (16)$$

$$\mu_{3/2} = \frac{x}{(1+x^{3/2})^{2/3}} [30] \rightarrow L_{3/2} = \frac{1}{1+x^{3/2}}. \quad (17)$$

The value of  $\eta$  depends on the Galactic field at the solar system's location which can be obtained from its centrifugal acceleration

$$A_{\text{cen}} = \frac{V^2}{R}, \quad (18)$$

where  $V$  is the speed of the Local Standard of Rest (LSR) and  $R = 8.5$  kpc is the Galactocentric distance. The standard IAU value for the speed is  $V = 220 \text{ km s}^{-1}$ , but recent determinations [32] obtained with the Very Long Baseline Array and the Japanese VLBI Exploration of Radio Astronomy project yield a higher value:  $V = 254 \pm 16 \text{ km s}^{-1}$ . Thus,  $\eta$  ranges from 1.5 to 2.3.

### 3 Orbits of Oort comets in MOND

#### 3.1 Ecliptic orbits

We will, now, consider an Oort comet whose Newtonian orbit covers the entire extension of the Oort cloud. It has semimajor axis  $a = 100$  kAU and eccentricity  $e = 0.5$ , so that its perihelion is 50 kAU and its aphelion is 150 kAU; for the sake of simplicity, we will assume it lies in the ecliptic plane. Its Newtonian orbital period is  $P_b = 31.6$  Myr. We will, first, use  $\eta = 2.0$  ( $V = 254 \text{ km s}^{-1}$ ) and  $\mu_{3/2}$ , so that

$$\mu_g = 0.82 \quad (19)$$

$$L_g = 0.25 \quad (20)$$

Figure 1 depicts the integrated Newtonian (dashed blue line) and MONDian (dash-dotted red line) orbits for the same initial conditions for  $-3P_b \leq t \leq 0$ . In Figure 2 we show the case  $\eta = 1.5$  ( $V = 220 \text{ km s}^{-1}$ ) yielding

$$\mu_g = 0.75 \quad (21)$$

$$L_g = 0.34. \quad (22)$$

The MOND trajectories are not closed and are much less spatially extended than the Newtonian ones; the overall shrinking of the orbit is more marked for the standard value of the LSR circular speed (Figure 2). Such an effect is particularly notable for highly elliptical Newtonian orbits, as shown by Figure 3- Figure 4 for  $e = 0.9$  and  $-P_b \leq t \leq 0$ . Note also how wildly the MOND trajectory changes during one Keplerian orbital period. In Figure

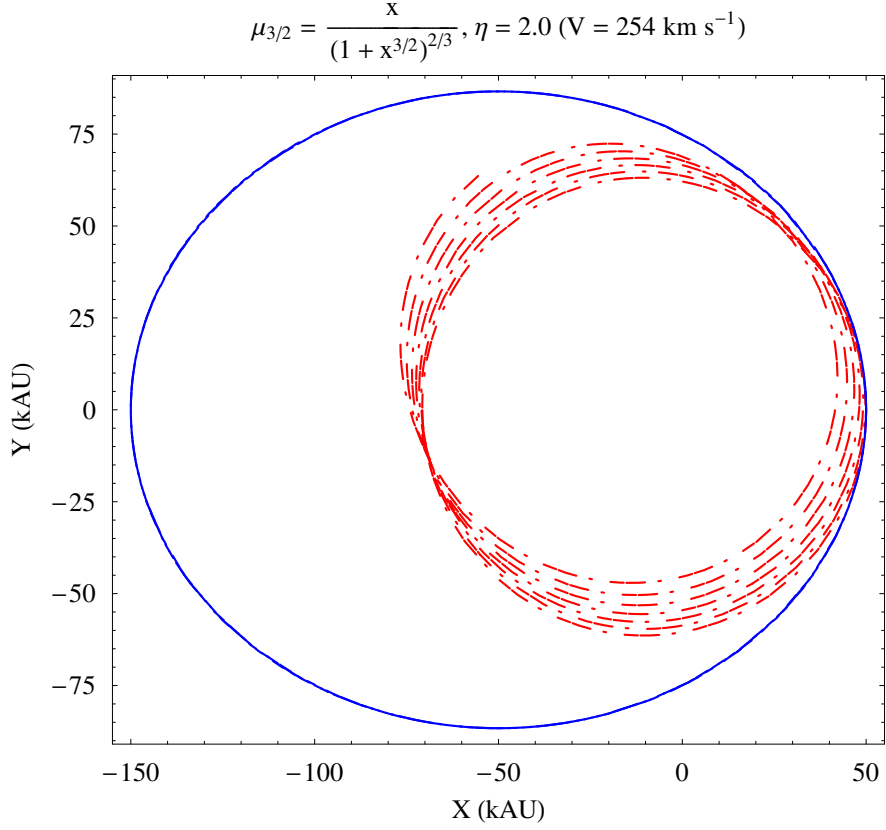


Figure 1: Numerically integrated orbits of an Oort comet with  $a = 100$  kAU,  $e = 0.5$ ,  $P_b = 31.6$  Myr. Dashed blue line: Newton. Dash-dotted red line: MOND with  $\mu_{3/2}$ ,  $\eta = 2.0$  ( $V = 254 \text{ km s}^{-1}$ ). The initial conditions are  $x_0 = a(1 - e)$ ,  $y_0 = z_0 = 0$ ,  $\dot{x}_0 = 0$ ,  $\dot{y}_0 = na\sqrt{\frac{1+e}{1-e}}$ ,  $\dot{z}_0 = 0$ . The time span of the integration is  $-3P_b \leq t \leq 0$ .

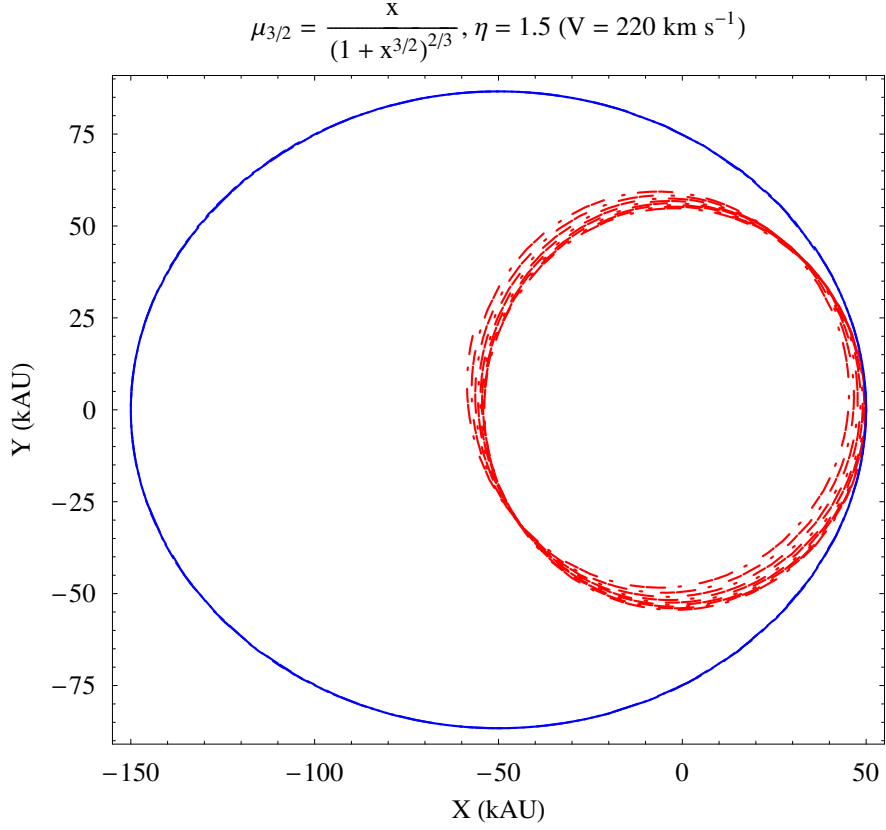


Figure 2: Numerically integrated orbits of an Oort comet with  $a = 100$  kAU,  $e = 0.5$ ,  $P_b = 31.6$  Myr. Dashed blue line: Newton. Dash-dotted red line: MOND with  $\mu_{3/2}$ ,  $\eta = 1.5$  ( $V = 220 \text{ km s}^{-1}$ ). The initial conditions are  $x_0 = a(1 - e)$ ,  $y_0 = z_0 = 0$ ,  $\dot{x}_0 = 0$ ,  $\dot{y}_0 = na\sqrt{\frac{1+e}{1-e}}$ ,  $\dot{z}_0 = 0$ . The time span of the integration is  $-3P_b \leq t \leq 0$ .

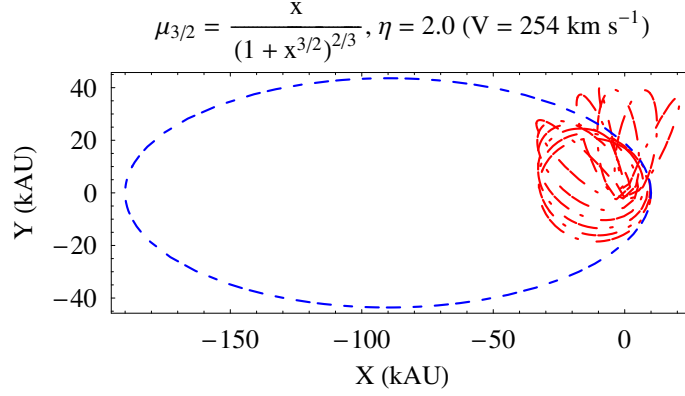


Figure 3: Numerically integrated orbits of an Oort comet with  $a = 100$  kAU,  $e = 0.9$ ,  $P_b = 31.6$  Myr. Dashed blue line: Newton. Dash-dotted red line: MOND with  $\mu_{3/2}$ ,  $\eta = 2.0$  ( $V = 254 \text{ km s}^{-1}$ ). The initial conditions are  $x_0 = a(1 - e)$ ,  $y_0 = z_0 = 0$ ,  $\dot{x}_0 = 0$ ,  $\dot{y}_0 = na\sqrt{\frac{1+e}{1-e}}$ ,  $\dot{z}_0 = 0$ . The time span of the integration is  $-P_b \leq t \leq 0$ .

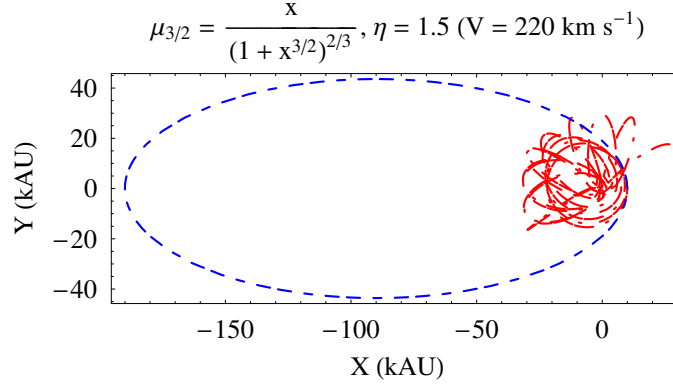


Figure 4: Numerically integrated orbits of an Oort comet with  $a = 100$  kAU,  $e = 0.9$ ,  $P_b = 31.6$  Myr. Dashed blue line: Newton. Dash-dotted red line: MOND with  $\mu_{3/2}$ ,  $\eta = 1.5$  ( $V = 220 \text{ km s}^{-1}$ ). The initial conditions are  $x_0 = a(1 - e)$ ,  $y_0 = z_0 = 0$ ,  $\dot{x}_0 = 0$ ,  $\dot{y}_0 = na\sqrt{\frac{1+e}{1-e}}$ ,  $\dot{z}_0 = 0$ . The time span of the integration is  $-P_b \leq t \leq 0$ .

5-Figure 8 we use  $\mu_2$ . The values of the MONDian characteristic parameters are

$$\mu_g = 0.89 \quad (23)$$

$$L_g = 0.19 \quad (24)$$

for  $\eta = 2.0$ , and

$$\mu_g = 0.83 \quad (25)$$

$$L_g = 0.29 \quad (26)$$

for  $\eta = 1.5$ . Also with such a form of the interpolating function  $\mu$ , orbits that are highly eccentric in Newtonian dynamics are confined to much smaller spatial regions in MOND and experience high-frequency variations over one Keplerian orbital period. However, for  $\mu_2$  the largest extension of the MOND trajectory occurs for  $V = 220 \text{ km s}^{-1}$  ( $\eta = 1.5$ ).

Let us, now, examine the case  $\mu_1$ . In Figure 9 we show the trajectory due to it of the Oort comet with  $e = 0.5$  over  $3P_b$  for  $\eta = 2.0$  which implies

$$\mu_g = 0.67 \quad (27)$$

$$L_g = 0.33. \quad (28)$$

The case  $\eta = 1.5$ , yielding

$$\mu_g = 0.60 \quad (29)$$

$$L_g = 0.39, \quad (30)$$

is shown in Figure 10 for  $-P_b \leq t \leq 0$ . The case of highly elliptic orbits ( $e = 0.9$ ) is more intricate, as shown by Figure 11 and Figure 12. The MOND paths resemble confuse clouds confined within a small spatial region.

The general features common to all the pictures shown may have consequences on the interaction of the Oort-like objects lying close to the ecliptic with passing stars [21] by reducing their perturbing effects and, thus, also altering the number of long-period comets launched into the inner regions of the Solar System, the number of comets left in the cloud throughout its history. Indeed, in the standard picture, the comets moving along very (Newtonian) elongated orbits may come relatively close to a star of mass  $M_\star$  suffering a change in velocity  $\Delta v$  which approximately is [21]

$$\Delta v = \frac{2GM_\star}{v_\star d}, \quad (31)$$

where  $v_\star$  is the star's velocity with respect to the Sun and  $d$  is the distance of closest approach with the Oort object. Moreover, less elongated orbits would also reduce the perturbing effects of the Galactic tides.

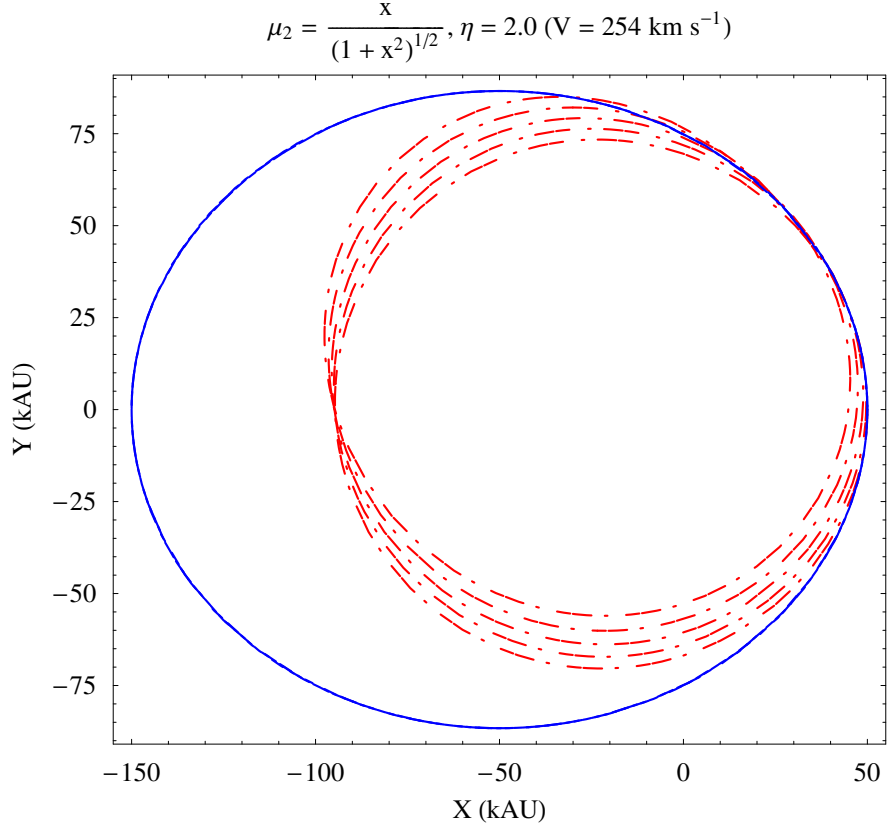


Figure 5: Numerically integrated orbits of an Oort comet with  $a = 100$  kAU,  $e = 0.5$ ,  $P_b = 31.6$  Myr. Dashed blue line: Newton. Dash-dotted red line: MOND with  $\mu_2, \eta = 2.0$  ( $V = 254 \text{ km s}^{-1}$ ). The initial conditions are  $x_0 = a(1 - e), y_0 = z_0 = 0, \dot{x}_0 = 0, \dot{y}_0 = na\sqrt{\frac{1+e}{1-e}}, \dot{z}_0 = 0$ . The time span of the integration is  $-3P_b \leq t \leq 0$ .

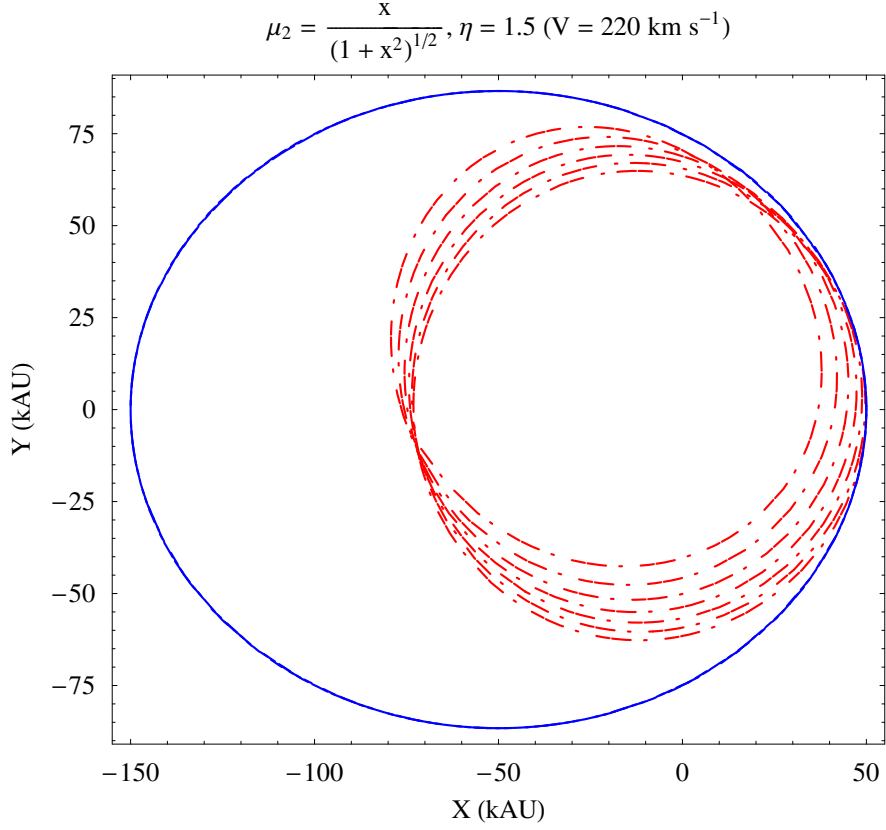


Figure 6: Numerically integrated orbits of an Oort comet with  $a = 100$  kAU,  $e = 0.5$ ,  $P_b = 31.6$  Myr. Dashed blue line: Newton. Dash-dotted red line: MOND with  $\mu_2, \eta = 1.5$  ( $V = 220$  km s $^{-1}$ ). The initial conditions are  $x_0 = a(1 - e), y_0 = z_0 = 0, \dot{x}_0 = 0, \dot{y}_0 = na\sqrt{\frac{1+e}{1-e}}, \dot{z}_0 = 0$ . The time span of the integration is  $-3P_b \leq t \leq 0$ .

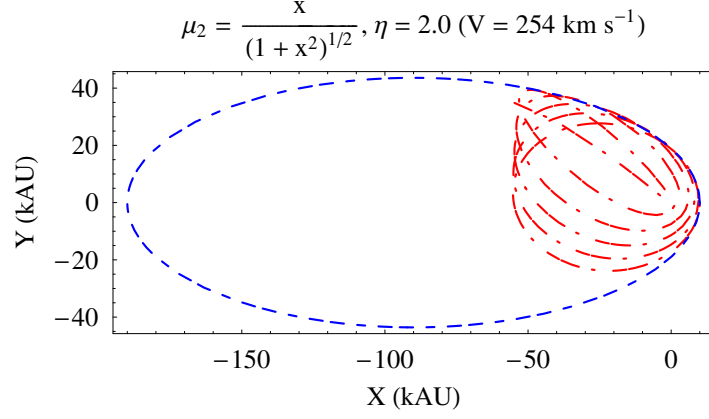


Figure 7: Numerically integrated orbits of an Oort comet with  $a = 100$  kAU,  $e = 0.9$ ,  $P_b = 31.6$  Myr. Dashed blue line: Newton. Dash-dotted red line: MOND with  $\mu_2, \eta = 2.0$  ( $V = 254$  km s $^{-1}$ ). The initial conditions are  $x_0 = a(1 - e), y_0 = z_0 = 0, \dot{x}_0 = 0, \dot{y}_0 = na\sqrt{\frac{1+e}{1-e}}, \dot{z}_0 = 0$ . The time span of the integration is  $-P_b \leq t \leq 0$ .

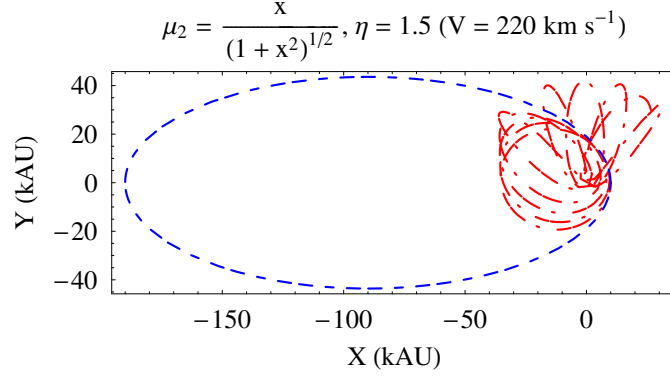


Figure 8: Numerically integrated orbits of an Oort comet with  $a = 100$  kAU,  $e = 0.9$ ,  $P_b = 31.6$  Myr. Dashed blue line: Newton. Dash-dotted red line: MOND with  $\mu_2, \eta = 1.5$  ( $V = 220$  km s $^{-1}$ ). The initial conditions are  $x_0 = a(1 - e), y_0 = z_0 = 0, \dot{x}_0 = 0, \dot{y}_0 = na\sqrt{\frac{1+e}{1-e}}, \dot{z}_0 = 0$ . The time span of the integration is  $-P_b \leq t \leq 0$ .

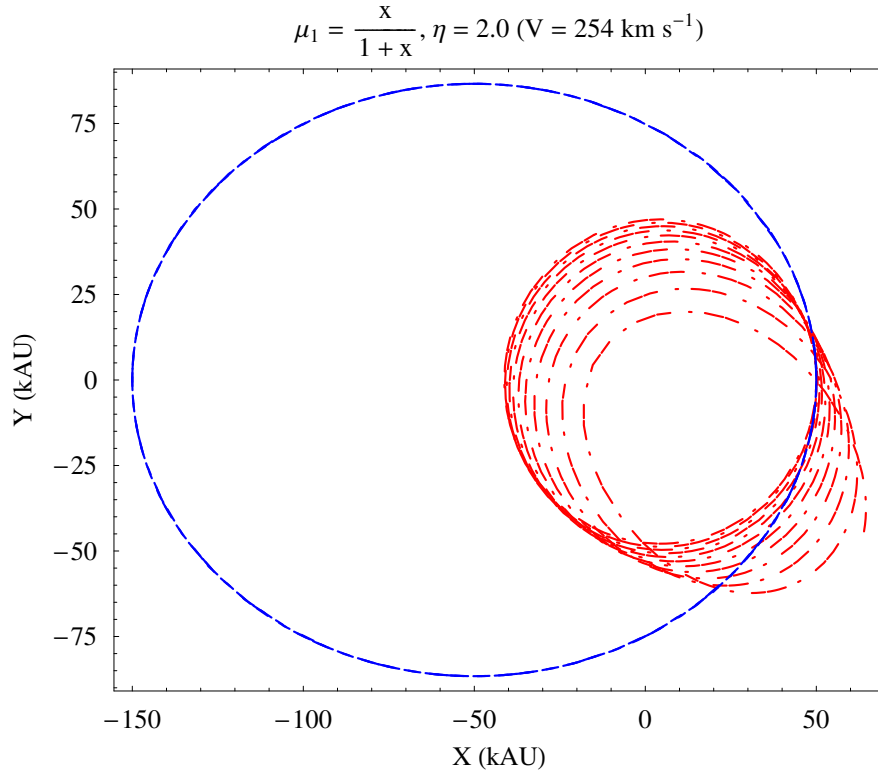


Figure 9: Numerically integrated orbits of an Oort comet with  $a = 100$  kAU,  $e = 0.5$ ,  $P_b = 31.6$  Myr. Dashed blue line: Newton. Dash-dotted red line: MOND with  $\mu_1, \eta = 2.0$  ( $V = 254 \text{ km s}^{-1}$ ). The initial conditions are  $x_0 = a(1 - e), y_0 = z_0 = 0, \dot{x}_0 = 0, \dot{y}_0 = na\sqrt{\frac{1+e}{1-e}}, \dot{z}_0 = 0$ . The time span of the integration is  $-3P_b \leq t \leq 0$ .

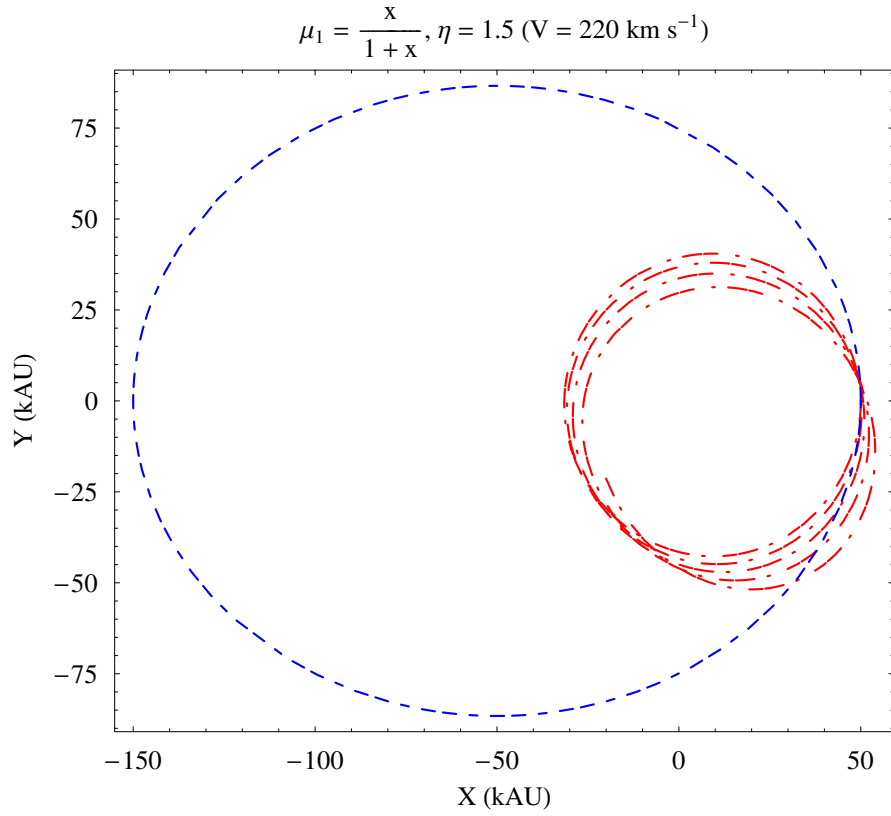


Figure 10: Numerically integrated orbits of an Oort comet with  $a = 100$  kAU,  $e = 0.5$ ,  $P_b = 31.6$  Myr. Continuous blue line: Newton. Dash-dotted red line: MOND with  $\mu_1$ ,  $\eta = 1.5$  ( $V = 220$  km s $^{-1}$ ). The initial conditions are  $x_0 = a(1 - e)$ ,  $y_0 = z_0 = 0$ ,  $\dot{x}_0 = 0$ ,  $\dot{y}_0 = na\sqrt{\frac{1+e}{1-e}}$ ,  $\dot{z}_0 = 0$ . The time span of the integration is  $-P_b \leq t \leq 0$ .

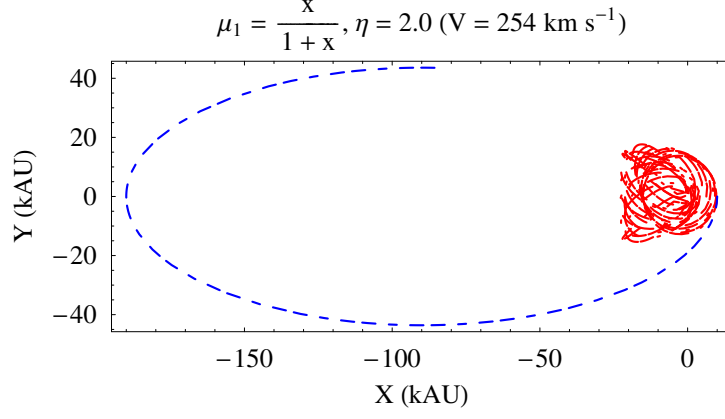


Figure 11: Numerically integrated orbits of an Oort comet with  $a = 100$  kAU,  $e = 0.9$ ,  $P_b = 31.6$  Myr. Dashed blue line: Newton. Dash-dotted red line: MOND with  $\mu_1$ ,  $\eta = 2.0$  ( $V = 254$  km s $^{-1}$ ). The initial conditions are  $x_0 = a(1 - e)$ ,  $y_0 = z_0 = 0$ ,  $\dot{x}_0 = 0$ ,  $\dot{y}_0 = na\sqrt{\frac{1+e}{1-e}}$ ,  $\dot{z}_0 = 0$ . The time span of the integration is  $-0.9P_b \leq t \leq 0$ .

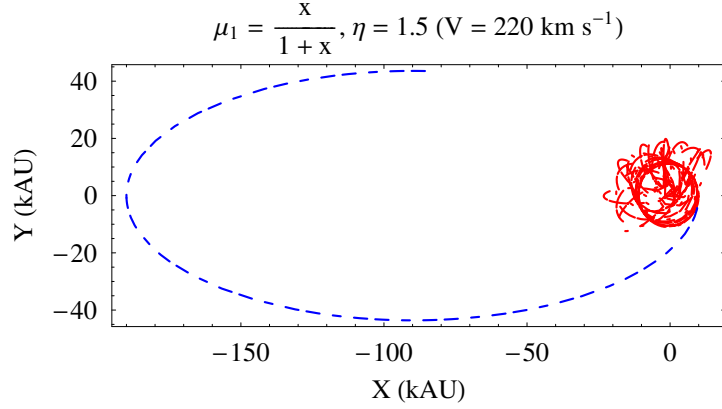


Figure 12: Numerically integrated orbits of an Oort comet with  $a = 100$  kAU,  $e = 0.9$ ,  $P_b = 31.6$  Myr. Dashed blue line: Newton. Dash-dotted red line: MOND with  $\mu_1$ ,  $\eta = 1.5$  ( $V = 220$  km s $^{-1}$ ). The initial conditions are  $x_0 = a(1 - e)$ ,  $y_0 = z_0 = 0$ ,  $\dot{x}_0 = 0$ ,  $\dot{y}_0 = na\sqrt{\frac{1+e}{1-e}}$ ,  $\dot{z}_0 = 0$ . The time span of the integration is  $-0.9P_b \leq t \leq 0$ .

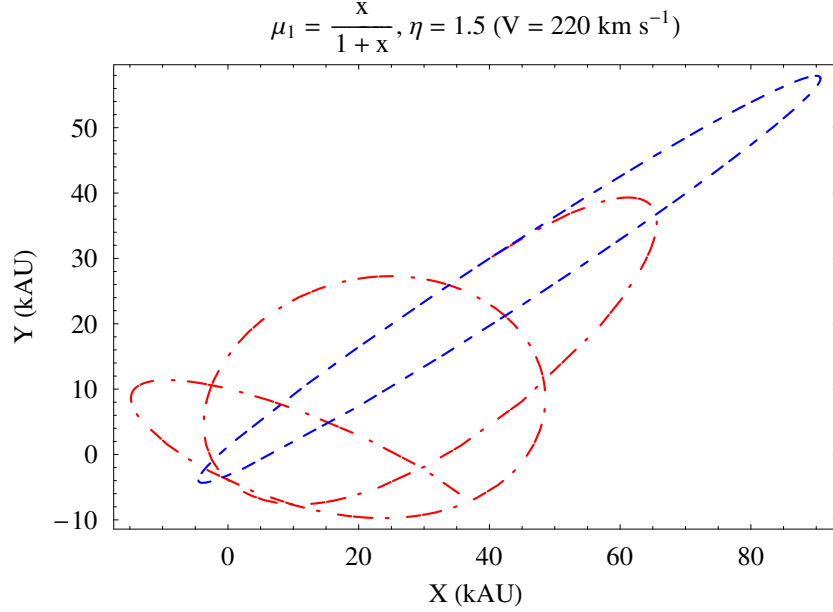


Figure 13: Section in the coordinate  $\{XY\}$  plane of the numerically integrated orbits of an Oort comet with  $a = 66.6$  kAU,  $e = 0.92$ ,  $I = 81$  deg. Dashed blue line: Newton. Dash-dotted red line: MOND with  $\mu_1, \eta = 1.5$  ( $V = 220 \text{ km s}^{-1}$ ). The initial conditions are  $x_0 = 40$  kAU,  $y_0 = 30$  kAU,  $z_0 = 5$  kAU,  $\dot{x}_0 = -23 \text{ kAU Myr}^{-1}$ ,  $\dot{y}_0 = -15 \text{ kAU Myr}^{-1}$ ,  $\dot{z}_0 = -15 \text{ kAU Myr}^{-1}$ . The time span of the integration is  $-P_b \leq t \leq 0$ .

### 3.2 Nearly polar orbits

Let us, now consider the case of orbits showing high inclinations  $I$  to the ecliptic. For space reasons we will only show some cases. In Figure 13-Figure 15 we depict the sections in the coordinate planes of an orbit with  $a = 66.6$  kAU,  $e = 0.92$ ,  $I = 81$  deg for  $\mu_1$  and  $\eta = 1.5$ . The case of  $\mu_2$  and  $\eta = 1.5$  is illustrated in Figure 16- Figure 18.

## 4 Summary and conclusions

We have numerically investigated the orbital motions of test particles according to MOND (with EFE) in the Oort cloud ( $r \approx 50 - 150$  kAU). As MONDian interpolating function  $\mu(x)$ , we extensively used the forms  $\mu_1 = 1/(1+x)$ ,  $\mu_2 = x/\sqrt{1+x^2}$ ,  $\mu_{3/2} = x/(1+x^{3/2})^{2/3}$ . We integrated both the MOND and the Newtonian equations of motion in Cartesian coordinates sharing the same initial conditions. We considered both ecliptic and nearly

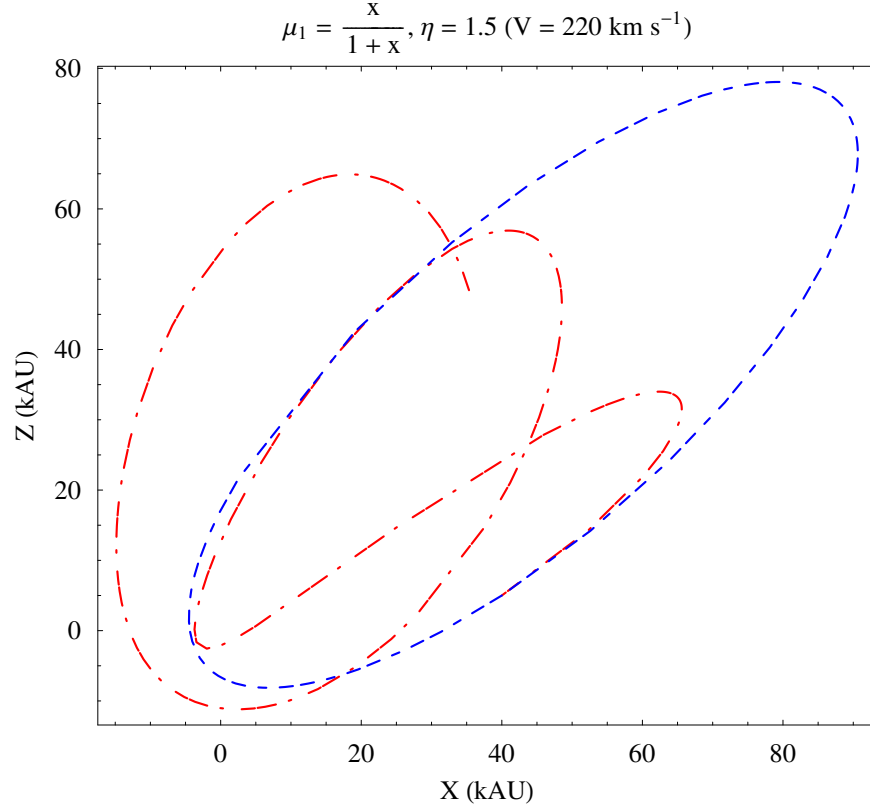


Figure 14: Section in the coordinate  $\{XZ\}$  plane of the numerically integrated orbits of an Oort comet with  $a = 66.6$  kAU,  $e = 0.92$ ,  $I = 81$  deg. Dashed blue line: Newton. Dash-dotted red line: MOND with  $\mu_1, \eta = 1.5$  ( $V = 220 \text{ km s}^{-1}$ ). The initial conditions are  $x_0 = 40$  kAU,  $y_0 = 30$  kAU,  $z_0 = 5$  kAU,  $\dot{x}_0 = -23$  kAU Myr $^{-1}$ ,  $\dot{y}_0 = -15$  kAU Myr $^{-1}$ ,  $\dot{z}_0 = -15$  kAU Myr $^{-1}$ . The time span of the integration is  $-P_b \leq t \leq 0$ .

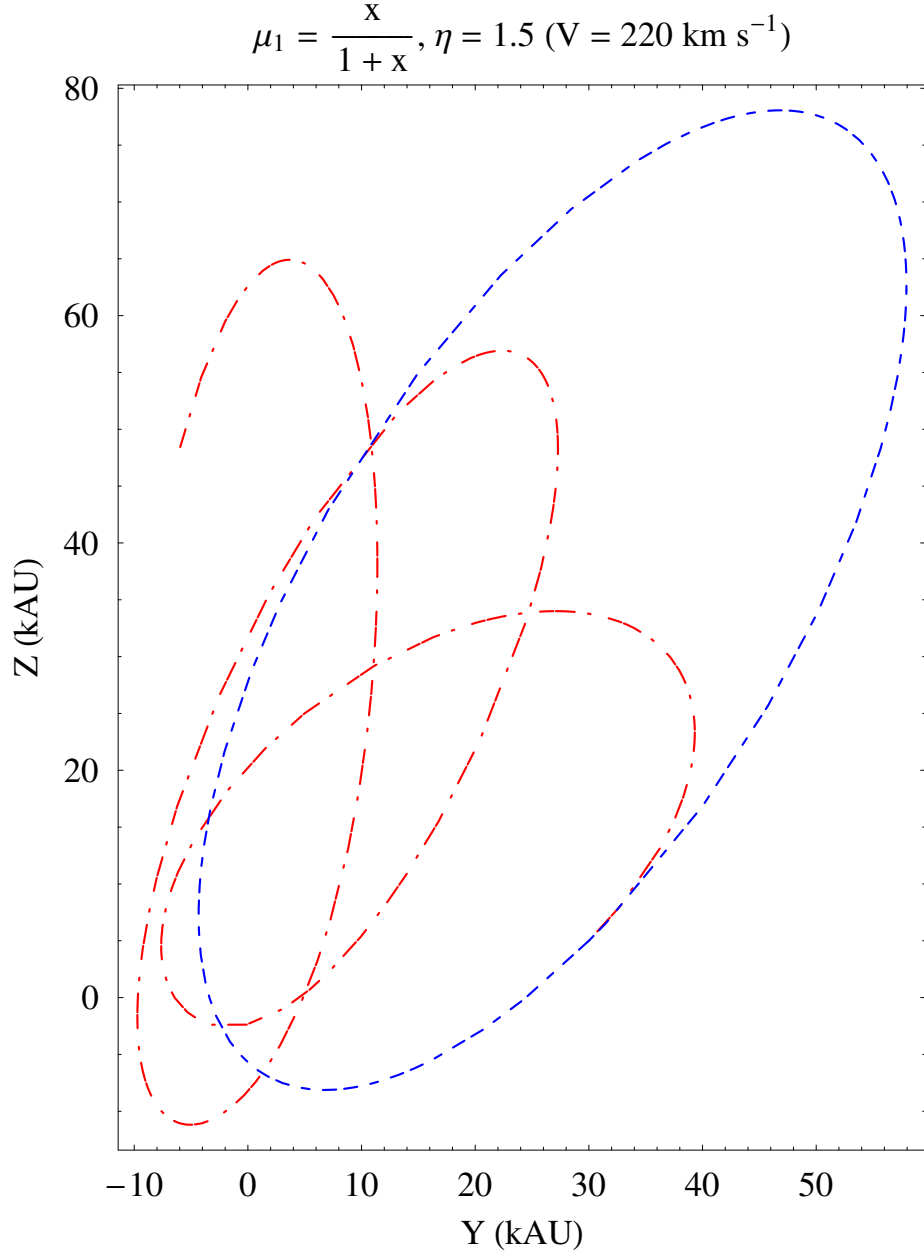


Figure 15: Section in the coordinate  $\{YZ\}$  plane of the numerically integrated orbits of an Oort comet with  $a = 66.6$  kAU,  $e = 0.92$ ,  $I = 81$  deg. Dashed blue line: Newton. Dash-dotted red line: MOND with  $\mu_1, \eta = 1.5$  ( $V = 220 \text{ km s}^{-1}$ ). The initial conditions are  $x_0 = 40$  kAU,  $y_0 = 30$  kAU,  $z_0 = 5$  kAU,  $\dot{x}_0 = -23 \text{ kAU Myr}^{-1}$ ,  $\dot{y}_0 = -15 \text{ kAU Myr}^{-1}$ ,  $\dot{z}_0 = -15 \text{ kAU Myr}^{-1}$ . The time span of the integration is  $-P_b \leq t \leq 0$ .

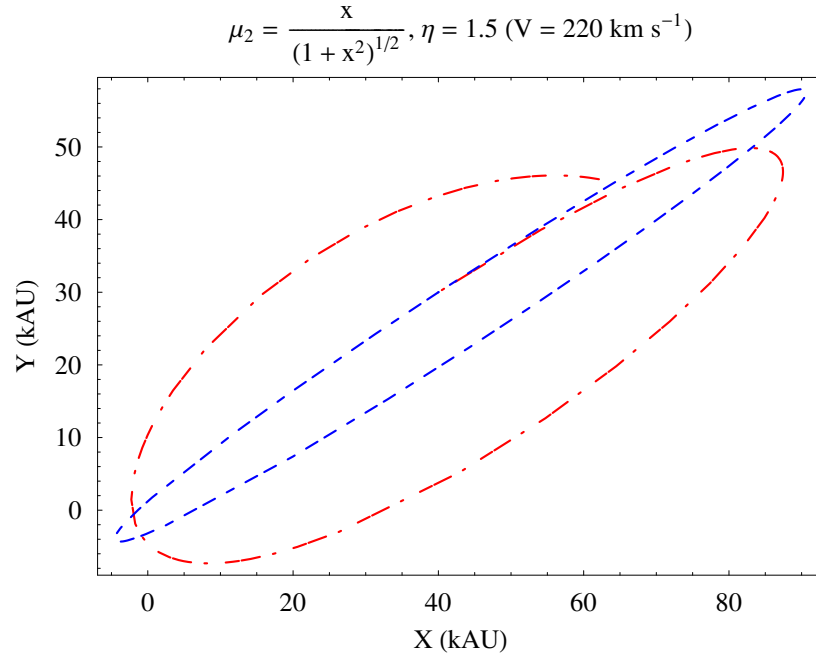


Figure 16: Section in the coordinate  $\{XY\}$  plane of the numerically integrated orbits of an Oort comet with  $a = 66.6$  kAU,  $e = 0.92$ ,  $I = 81$  deg. Dashed blue line: Newton. Dash-dotted red line: MOND with  $\mu_2, \eta = 1.5$  ( $V = 220 \text{ km s}^{-1}$ ). The initial conditions are  $x_0 = 40$  kAU,  $y_0 = 30$  kAU,  $z_0 = 5$  kAU,  $\dot{x}_0 = -23 \text{ kAU Myr}^{-1}$ ,  $\dot{y}_0 = -15 \text{ kAU Myr}^{-1}$ ,  $\dot{z}_0 = -15 \text{ kAU Myr}^{-1}$ . The time span of the integration is  $-P_b \leq t \leq 0$ .

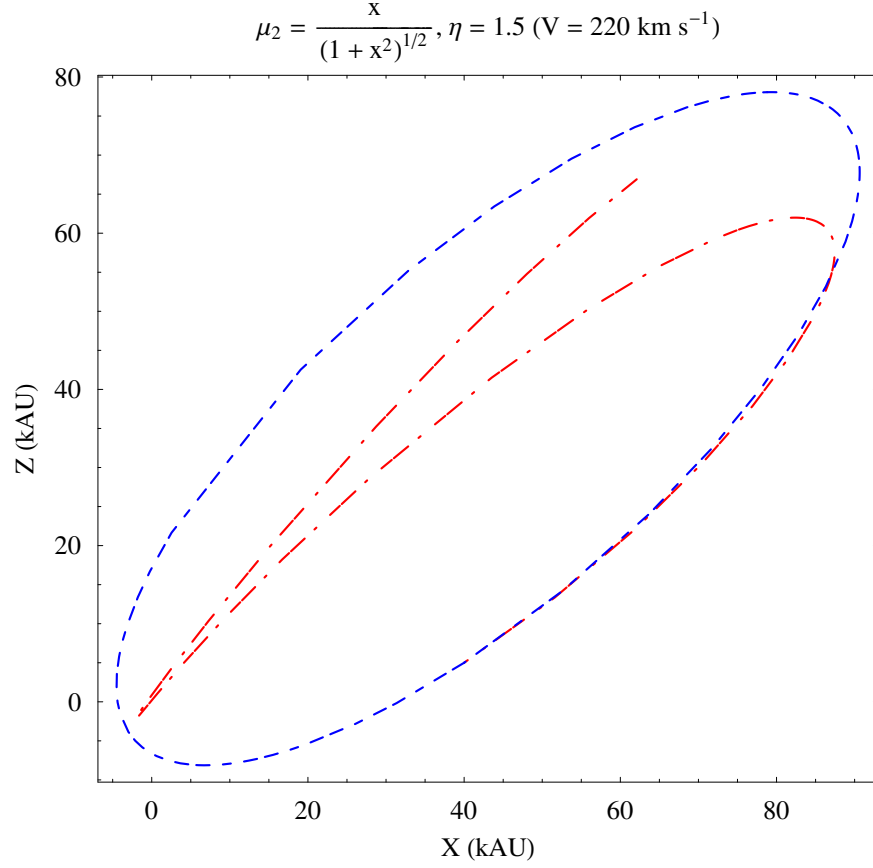


Figure 17: Section in the coordinate  $\{XZ\}$  plane of the numerically integrated orbits of an Oort comet with  $a = 66.6$  kAU,  $e = 0.92$ ,  $I = 81$  deg. Dashed blue line: Newton. Dash-dotted red line: MOND with  $\mu_2, \eta = 1.5$  ( $V = 220 \text{ km s}^{-1}$ ). The initial conditions are  $x_0 = 40$  kAU,  $y_0 = 30$  kAU,  $z_0 = 5$  kAU,  $\dot{x}_0 = -23 \text{ kAU Myr}^{-1}$ ,  $\dot{y}_0 = -15 \text{ kAU Myr}^{-1}$ ,  $\dot{z}_0 = -15 \text{ kAU Myr}^{-1}$ . The time span of the integration is  $-P_b \leq t \leq 0$ .

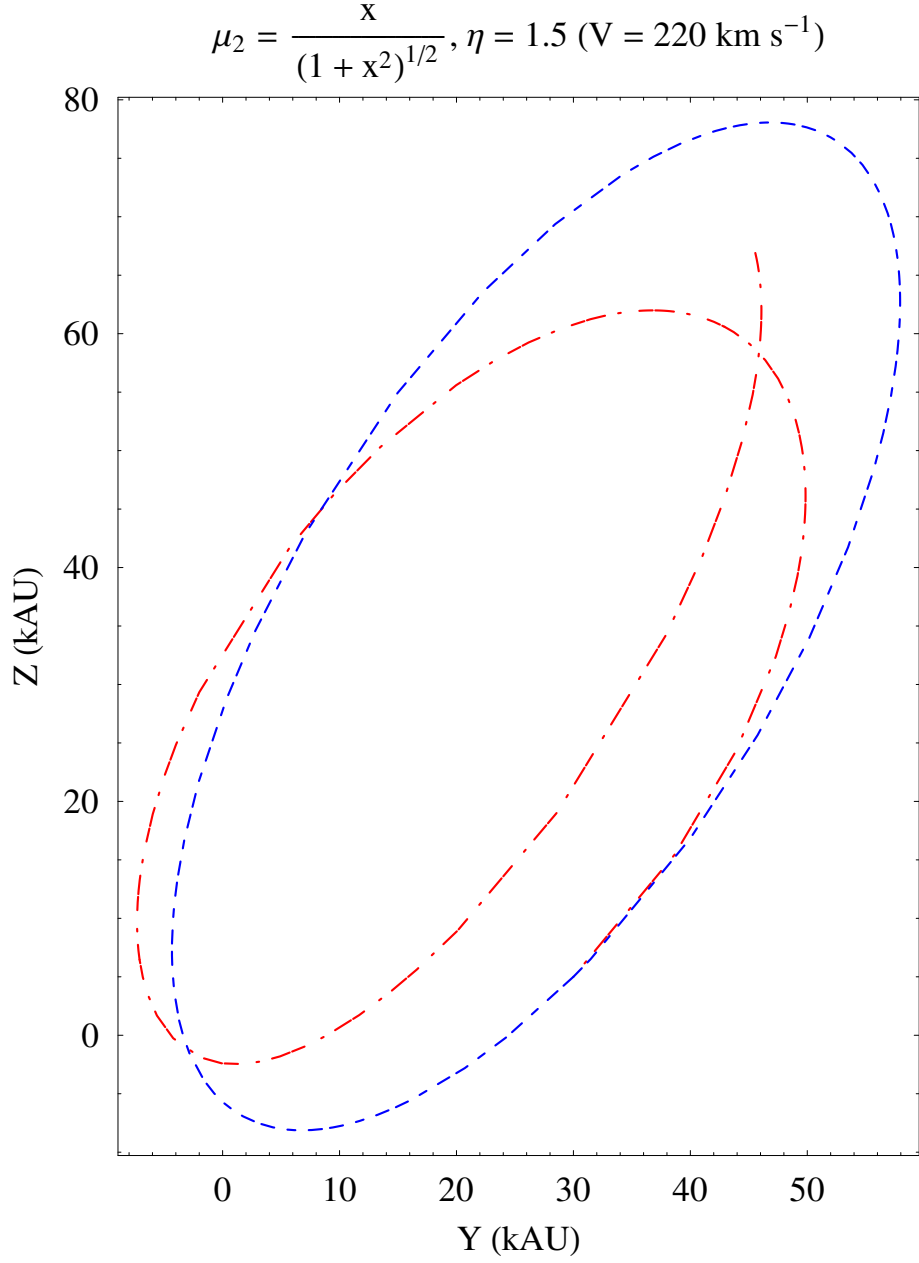


Figure 18: Section in the coordinate  $\{YZ\}$  plane of the numerically integrated orbits of an Oort comet with  $a = 66.6$  kAU,  $e = 0.92$ ,  $I = 81$  deg. Dashed blue line: Newton. Dash-dotted red line: MOND with  $\mu_2, \eta = 1.5$  ( $V = 220 \text{ km s}^{-1}$ ). The initial conditions are  $x_0 = 40$  kAU,  $y_0 = 30$  kAU,  $z_0 = 5$  kAU,  $\dot{x}_0 = -23 \text{ kAU Myr}^{-1}$ ,  $\dot{y}_0 = -15 \text{ kAU Myr}^{-1}$ ,  $\dot{z}_0 = -15 \text{ kAU Myr}^{-1}$ . The time span of the integration is  $-P_b \leq t \leq 0$ .

polar trajectories, all with high eccentricities. In order to evaluate the characteristic MOND parameters  $\mu_g$  and  $L_g$  entering the problem, we used two different values ( $V = 220 \text{ km s}^{-1}$  and  $V = 254 \text{ km s}^{-1}$ ) of the circular speed of the solar system's motion through the Galaxy yielding the Milky Way's gravitational field at the Sun's location.

The structure and the dynamical history of the Oort cloud, in deep MONDian regime, would be altered with respect to the standard Newtonian picture because highly eccentric orbits would not be allowed in the ecliptic plane by MOND which, on the contrary, strongly tends to shrink them. As a consequence, one may speculate that the number of long-period comets launched in the inner parts of the Solar System should be reduced because of the less effective perturbing actions of nearby passing stars, interstellar clouds and Galactic tides. Out of the ecliptic the situation is different because, although distorted with respect to the Newtonian case, the MOND orbits tend to occupy not so smaller spatial regions.

## References

- [1] A. Bosma, "21-cm line studies of spiral galaxies. I - Observations of the galaxies NGC 5033, 3198, 5055, 2841, and 7331. II - The distribution and kinematics of neutral hydrogen in spiral galaxies of various morphological types", *The Astronomical Journal*, vol. 86, December 1981, pp. 1791-1846, 1981.
- [2] V. C. Rubin, W. K. Ford, N. Thonnard, and D. Burstein, "Rotational properties of 23 SB galaxies", *The Astrophysical Journal*, vol. 261, October 15, pp. 439-456, 1982.
- [3] V. C. Rubin, "The Rotation of Spiral Galaxies", *Science*, vol. 220, no. 4604, pp. 1339-1344, 1983.
- [4] M. Milgrom, "A Modification of the Newtonian Dynamics as a Possible Alternative to the Hidden Mass Hypothesis", *The Astrophysical Journal*, vol. 270, July 15, pp. 365-370, 1983a.
- [5] M. Milgrom, "A Modification of the Newtonian Dynamics - Implications for Galaxies", *The Astrophysical Journal*, vol. 270, July 15, pp. 371-389, 1983b.
- [6] M. Milgrom, "A Modification of the Newtonian Dynamics - Implications for Galaxy Systems", *The Astrophysical Journal*, vol. 270, July 15, pp. 384-389, 1983c.

- [7] K. G. Begeman, A. H. Broeils, and R. H. Sanders, “Extended rotation curves of spiral galaxies - Dark haloes and modified dynamics”, *Monthly Notices of the Royal Astronomical Society*, vol. 249, April 1, pp. 523-537, 1991.
- [8] B. Famaey, and J. Binney, “Modified Newtonian dynamics in the Milky Way”, *Monthly Notices of the Royal Astronomical Society*, vol. 363, no. 2, pp. 603-608, 2005.
- [9] J. D. Bekenstein, and M. Milgrom, “Does the Missing Mass Problem Signal the Breakdown of Newtonian Gravity?”, *The Astrophysical Journal*, vol. 286, November 1, pp. 7-14, 1984.
- [10] H. Zhao, and B. Famaey, “Refining the MOND Interpolating Function and TeVeS Lagrangian”, *The Astrophysical Journal*, vol. 638, no. 1, pp. L9-L12, 2006.
- [11] B. Famaey, G. Gentile, J.-P. Bruneton, and H. Zhao, “Insight into the baryon-gravity relation in galaxies”, *Physical Review D*, vol. 75, no. 6, Article ID 063002, 15 pages, 2007.
- [12] R. H. Sanders, and E. Noordermeer, “Confrontation of MOdified Newtonian Dynamics with the rotation curves of early-type disc galaxies”, *Monthly Notices of the Royal Astronomical Society*, vol. 379, no. 2, pp. 702-710, 2007.
- [13] R. Brada, and M. Milgrom, “Exact solutions and approximations of MOND fields of disc galaxies”, *Monthly Notices of the Royal Astronomical Society*, vol. 276, no. 2, pp. 453-459, 1995.
- [14] J. D. Bekenstein, “Relativistic gravitation theory for the modified Newtonian dynamics paradigm”, *Physical Review D*, vol. 70, no. 8, Article ID 083509, 28 pages, 2004.
- [15] J.-P. Bruneton, and G. Esposito-Farèse, “Field-theoretical formulations of MOND-like gravity”, *Physical Review D*, vol. 76, no. 12, Article ID 124012, 41 pages, 2007.
- [16] H. Zhao, “Coincidences of Dark Energy with Dark Matter: Clues for a Simple Alternative?”, *The Astrophysical Journal*, vol. 671, no. 1, pp. L1-L4, 2007.
- [17] L. Iorio, “On the MOND external field effect in the solar system ”, *Astrophysics and Space Science*, doi:10.1007/s10509-009-0061-3, 2009.

- [18] R. H. Sanders, and S. S. McGaugh, “Modified Newtonian Dynamics as an Alternative to Dark Matter”, *Annual Review of Astronomy and Astrophysics*, vol. 40, September 2002, pp. 263-317, 2002.
- [19] J. D. Bekenstein, “The modified Newtonian dynamics - MOND and its implications for new physics”, *Contemporary Physics*, vol. 47, no. 6, pp. 387-403, 2006.
- [20] M. Milgrom, “The MOND paradigm”, Talk presented at the xIx Rencontres de Blois “Matter and energy in the Universe: from nucleosynthesis to cosmology”, May 2007, <http://arxiv.org/abs/0801.3133v2>.
- [21] J. H. Oort, “The structure of the cloud of comets surrounding the solar system and a hypothesis concerning its origin”, *Bullettin of the Astronomical Institutes of The Netherlands*, vol. 11, no. 408, pp. 91-110, 1950.
- [22] M. Milgrom, “Solutions for the modified Newtonian dynamics field equation”, *The Astrophysical Journal*, vol. 302, March 15, pp. 617-625, 1986.
- [23] C. Talmadge, J.-P. Berthias, R. W. Hellings, and E. M. Standish, “Model-independent constraints on possible modifications of Newtonian gravity”, *Physical Review Letters*, vol. 61, no. 10, pp. 1159-1162, 1988.
- [24] M. Sereno, and Ph. Jetzer, “Dark matter versus modifications of the gravitational inverse-square law: results from planetary motion in the solar system”, *Monthly Notices of the Royal Astronomical Society*, vol. 371, no. 2, pp. 626-632, 2006.
- [25] J. D. Bekenstein, and J. Magueijo, “Modified Newtonian dynamics habitats within the solar system”, *Physical Review D*, vol. 73, no. 10, Article ID 103513, 14 pages, 2006.
- [26] R. H. Sanders, “solar system constraints on multifield theories of modified dynamics”, *Monthly Notices of the Royal Astronomical Society*, vol. 370, no. 3, pp. 1519-1528, 2006.
- [27] A. Yu. Ignatiev, “Is Violation of Newton’s Second Law Possible?”, *Physical Review Letters*, vol. 98, no. 10, Article ID 101101, 4 pages, 2007.
- [28] L. Iorio, “Constraining MOND with solar system dynamics”, *Journal of Gravitational Physics*, vol. 2, no. 1, pp. 26-32, 2008.

- [29] A. Yu. Ignatiev, “Newton’s second law versus modified-inertia MOND: A test using the high-latitude effect”, *Physical Review D*, vol. 77, no. 10, Article ID 102001, 9 pages, 2008.
- [30] M. Milgrom, “MOND effects in the inner solar system”, *Monthly Notices of the Royal Astronomical Society*, at press, 2009. arXiv:0906.4817v1
- [31] L. Iorio, “The perihelion precession of Saturn, planet x/Nemesis and MOND”, 2009b. arXiv:0907.4514v1
- [32] M. J. Reid, K. M. Menten, X. W. Zheng, A. Brunthaler, L. Moscadelli, Y. Xu, B. Zhang, M. Sato, M. Honma, T. Hirota, K. Hachisuka, Y. K. Choi, G. A. Moellenbrock, A. Bartkiewicz, “Trigonometric Parallaxes of Massive Star Forming Regions: VI. Galactic Structure, Fundamental Parameters and Non-Circular Motions”, *The Astrophysical Journal*, vol. 700, no. 1, pp. 137-148, 2009.